


Central-moment-based Galilean-invariant multiple-relaxation-time collision modelXiaowen Shan (单肖文)^{*}*Shenzhen Key Laboratory of Complex Aerospace Flows, Department of Mechanic and Aerospace Engineering, Southern University of Science and Technology, Shenzhen, Guangdong 518055, China* (Received 13 August 2018; revised manuscript received 11 September 2019; published 24 October 2019)

Aiming at systematically correcting the non-Galilean-invariant thermal diffusivity in the previous multiple-relaxation-time Boltzmann equation collision model [Shan and Chen, *Int. J. Mod. Phys. C* **18**, 635 (2007)], we show that by separately relaxing the central moments of the distribution function, Chapman-Enskog calculation leads to the correct hydrodynamic equations with mutually independent and Galilean invariant viscosity and thermal diffusivity, provided the velocity-space discretization preserves moments up to the fourth order. By transforming the central moments back to the absolute reference frame and evaluating using fixed discrete velocities, the efficient and accurate streaming-collision time-stepping algorithm is preserved. The lattice Boltzmann model is found to have excellent numerical stability in high-Reynolds-number simulations.

DOI: [10.1103/PhysRevE.100.043308](https://doi.org/10.1103/PhysRevE.100.043308)**I. INTRODUCTION**

In the past three decades the lattice Boltzmann method (LBM) [1–3], particularly the lattice Bhatnagar-Gross-Krook (LBGK) single-relaxation-time (SRT) model [4–6], has gained tremendous popularity in many areas of fluid mechanics. Despite great success, a number of deficiencies have long plagued LBGK. The most noticeable ones are perhaps the fixed unity Prandtl number, the sometimes poor numerical stability, and the various forms of violations of Galilean invariance. Aiming at eliminating, or at least alleviating, these deficiencies, a number of efforts have been made to improve the collision model, including the multiple-relaxation-time (MRT) model [7,8] and its central-moment (CM) version [9], the “regularized” models [10–13], and the Hermite expansion-based high-order MRT model [14,15]. These models, suggested with their own purposes and assumptions, all enjoyed success of various degrees and shared the commonality that the moments of the distribution are individually manipulated. One of the aims of the present work is to offer a coherent view that can hopefully provide a theoretical framework within which the essence of the aforementioned models can be examined.

The unity Prandtl number is a well-known artifact of the BGK model which relaxes all moments at the same rate. A few remedies in continuum, e.g., the model of Gross and Jackson [16], the ellipsoid-statistical BGK [17,18], and the Shakhov model [19], were suggested to introduce additional parameters in the target distribution to decouple the heat flux from stress. In the LB realm, McNamara *et al.* [20] implemented an LB collision operator with a different eigenvalue for the third moments with respect to the *peculiar velocity* to adjust the thermal conductivity. Nevertheless, it suffers from poor numerical stability due to, at least in part, the

insufficient lattice. d’Humières *et al.* [7,8] suggested an MRT model in which the distribution function is decomposed into eigenvectors corresponding to the lowest raw moments, and a separate relaxation time is assigned to each of them. Theoretically the model allows a variable Prandtl number. However, as recovery of the energy equation in LB requires a lattice with higher degree of symmetry than the ones on which the MRT was developed [21,22], the MRT was mostly advocated as a stability improvement. The idea of assigning separate relaxation times to the moments was generalized to obtain a high-order MRT (HMRT) model with variable Prandtl number [14]. A remaining problem is that the thermal diffusion is not Galilean invariant when the thermal diffusivity is different from the viscosity. More recently [15] this problem was also fixed *a posteriori* by modifying the equilibrium in a fashion similar to Ref. [5] to ensure that correct NSF equations are obtained. Nevertheless, it is not clear how this approach can be extended to the relaxation of higher-order moments.

The Galilean invariance problem refers to a class of non-physical defects originated from the lattice gas cellular automaton (LGA) fluid models [1]. Most of these problems were fixed in the LBGK model [5,6] except that the viscosity and thermal diffusivity unphysically depend on fluid velocity [21,23], which is widely known as the “cubic” error. This deviation is essentially due to insufficient accuracy when discretizing the BGK equation in velocity space and can be completely eliminated by using higher-order equilibrium and lattices [22]. Partial removal is also possible by explicitly correcting the incomplete third moments or using a velocity-dependent relaxation time [21,24]. The problem also exists in occasions such as the fluctuating LB models [25], where it was suggested that the relaxation should be done in the reference frame moving with the fluid.

The cascaded LB [9] (CLB) extends the MRT by relaxing the central moments (CMs), i.e., moments in the reference frame moving with the fluid. It has been observed in simulation that CLB has a drastically improved numerical stability

^{*}shanxw@sustech.edu.cn

over MRT [9,26], which is understandable as expansion in CM intrinsically has a faster convergence. Similarly to MRT, CLB formulation is lattice dependent and restricted to small lattices, which makes it difficult to be extended to high orders to allow a Galilean-invariant energy equation. More recently, a CM-based LB model for in-compressible thermal flows is proposed [27] to use a separate distribution for the energy equation. It was concluded that Galilean invariance was significantly improved but not fully restored due to the limitation of the underlying lattice.

In practical simulations, the MRT model was observed to drastically improve the numerical stability at high Reynolds numbers [8]. It is generally agreed that the improvement is due to the filtering of the “ghost” modes, i.e., the high-order tensors that are only partially represented by the discrete velocities. Similar improvements were indeed achieved by the “regularized” models which trim the unresolved moments [10,11,28]. More recently, the regularization approach was extended to high-order LB [12,13,29], leading to further enhanced numerical stability.

To directly compute the CMs with discrete velocities via quadrature rules, the abscissas must be chosen in the moving frame and become dependent on the hydrodynamic variables. Some kind of interpolation scheme must be adopted to reconcile the distributions on neighboring sites. Sun *et al.* [30,31] devised such an *adaptive* LB and fast convergence was indeed achieved. The downside is that the original simple streaming operation is complicated by the interpolation. If the efficient and accurate streaming-collision algorithm and linear advection are preferred, the discrete velocities must be fixed in the absolute frame.

In the present work, we show that the thermal diffusivity in HMRT [14] can be systematically made Galilean-invariant by separately relaxing the *central* moments instead of the raw ones. Taking advantage of the isomorphic transform between the Hermite coefficients and the discrete distribution function values established by Gauss integration when the distribution is restricted to the low-dimensional functional space span by the leading Hermite polynomials [32,33], the extraction of moments can be simple and lattice independent. This simplicity allows easy construction of a high-order CM-based MRT model with independent and Galilean-invariant viscous and thermal dissipation. The simple LB streaming-collision time stepping is preserved by evaluating the CMs from the raw moments *via* binomial transform. The current scheme agrees with Ref. [15] at the lowest order and can be extended to higher orders.

The work is organized as follows. The theoretical formulation is presented in Sec. II, where, after laying out necessary background, we first define a transform between the moments and the discrete distribution in Sec. II A. In Sec. II B some previous LB collision models are examined within this framework. In Sec. II C the general conditions for the collision term to yield NSF equations are obtained by examining the CE procedure with BGK collision operator [34,35]. Using these conditions, a generic high-order MRT collision model is then constructed in terms of its Hermite expansion. Numerical verifications are provided in Sec. III, and further discussions and conclusions are in Sec. IV. Some relations between the

moments and Hermite coefficients in the absolute and relative frames are given in Appendix.

II. THEORETICAL DERIVATION

The LB equation can be viewed as the projection of the following continuous Boltzmann-BGK equation into a low-dimensional Hilbert space spanned by the leading Hermite polynomials:

$$\frac{\partial f}{\partial t} + \boldsymbol{\xi} \cdot \nabla f + \mathbf{g} \cdot \nabla_{\boldsymbol{\xi}} f = \Omega(f). \quad (1)$$

Here f , $\boldsymbol{\xi}$, and \mathbf{g} are the single-particle distribution, the particle velocity, and the external body force, respectively; $\nabla_{\boldsymbol{\xi}}$ is the gradient operator in velocity space; and $\Omega(f)$ is the BGK single-relaxation-time (SRT) collision model [4]:

$$\Omega = -\frac{1}{\tau}[f - f^{(0)}], \quad (2)$$

and $f^{(0)}$ the Maxwellian:

$$f^{(0)} = \frac{\rho}{(2\pi\theta)^{D/2}} \exp\left[-\frac{|\boldsymbol{\xi} - \mathbf{u}|^2}{2\theta}\right], \quad (3)$$

where ρ , \mathbf{u} , and θ are, respectively, the dimensionless fluid density, velocity, and temperature [33].

Hermite polynomials in high dimensions were extensively treated by Grad [36]. Throughout the paper, we use a slightly different notation which is standard in tensor analysis. First define the *symmetrization* operator:

$$\text{Sym}(\mathbf{A}) \equiv \frac{1}{r!} \sum A_{i_1 \dots i_r}, \quad (4)$$

where \mathbf{A} is a rank- r tensor and the summation is over the $r!$ permutations of the r indexes. The *symmetric product* of two tensors, \mathbf{A} and \mathbf{B} , is denoted by \mathbf{AB} and defined as:

$$\mathbf{AB} \equiv \text{Sym}(\mathbf{A} \otimes \mathbf{B}), \quad (5)$$

where \otimes stands for the normal tensor product. The symmetric product has the following properties:

- (1) commutativity: $\mathbf{AB} = \mathbf{BA}$;
- (2) associativity: $(\mathbf{AB})\mathbf{C} = \mathbf{A}(\mathbf{BC})$;
- (3) distributivity: $(\mathbf{A} + \mathbf{B})\mathbf{C} = \mathbf{AC} + \mathbf{BC}$.

Hereinafter all tensor products are symmetric unless otherwise noted.

A. The discrete Hermite transform

Critical to our formulation of the MRT collision operator is the extraction of the velocity moments from the *discrete* distributions. Similarly to the discrete Fourier transforms (DFT), for a function that is a finite Hermite series, a transform between its moments and discrete function values can be defined via quadrature [37,38].

First, the Hermite polynomials form an orthonormal basis of the square-integrable functions in D dimensions with respect to the interproduct $\langle f, g \rangle \equiv \int \omega f g d\boldsymbol{\xi}$, where $\omega(\boldsymbol{\xi})$ is the weight function:

$$\frac{1}{(2\pi)^{D/2}} \exp\left[-\frac{|\boldsymbol{\xi}|^2}{2}\right]. \quad (6)$$

For any function f such that f/ω is square integrable, the following general Fourier series exists:

$$f(\boldsymbol{\xi}) = \omega(\boldsymbol{\xi}) \sum_{n=0}^{\infty} \frac{1}{n!} \mathbf{a}^{(n)} : \mathcal{H}^{(n)}(\boldsymbol{\xi}), \quad (7)$$

where “:” denotes full tensor contraction and

$$\mathbf{a}^{(n)} = \int f(\boldsymbol{\xi}) \mathcal{H}^{(n)}(\boldsymbol{\xi}) d\boldsymbol{\xi}, \quad n = 0, \dots, \infty, \quad (8)$$

is the n th Hermite coefficients. Since $\mathcal{H}^{(n)}(\boldsymbol{\xi})$ is a polynomial in $\boldsymbol{\xi}$, $\mathbf{a}^{(n)}$ are combinations of the velocity moments.

For an N th degree polynomial, $p_N(\boldsymbol{\xi})$, there exists a set of abscissas and associated weights, $\{\boldsymbol{\xi}_i, w_i : i = 1, \dots, d\}$, such that:

$$\int \omega(\boldsymbol{\xi}) p_N(\boldsymbol{\xi}) d\boldsymbol{\xi} = \sum_{i=1}^d w_i p_N(\boldsymbol{\xi}_i). \quad (9)$$

Particularly, quadrature rules with abscissas coincide with a Bravais lattice, or “on-lattice” quadratures, and can be obtained by solving a *linear programming* problem [33,39–42].

Consider the N th-order truncation of Eq. (7):

$$f_N(\boldsymbol{\xi}) \equiv \omega(\boldsymbol{\xi}) \sum_{n=0}^N \frac{1}{n!} \mathbf{a}^{(n)} : \mathcal{H}^{(n)}(\boldsymbol{\xi}), \quad (10)$$

where by Eq. (8), $\mathbf{a}^{(n)}$ are determined as:

$$\begin{aligned} \mathbf{a}^{(n)} &= \int f_N(\boldsymbol{\xi}) \mathcal{H}^{(n)}(\boldsymbol{\xi}) d\boldsymbol{\xi} \\ &= \int \omega(\boldsymbol{\xi}) \left[\frac{f_N(\boldsymbol{\xi}) \mathcal{H}^{(n)}(\boldsymbol{\xi})}{\omega(\boldsymbol{\xi})} \right] d\boldsymbol{\xi}. \end{aligned} \quad (11)$$

Note that the term inside the brackets is an $(N+n)$ -th degree polynomial. Letting $\boldsymbol{\xi}_i$ and w_i , $i = 1, \dots, d$, be the abscissas and weights of a degree- Q quadrature rule, by Eq. (9) we have:

$$\mathbf{a}^{(n)} = \sum_{i=1}^d f_i \mathcal{H}^{(n)}(\boldsymbol{\xi}_i), \quad \text{for } n = 0, \dots, Q - N, \quad (12)$$

where

$$f_i \equiv \frac{w_i f_N(\boldsymbol{\xi}_i)}{\omega(\boldsymbol{\xi}_i)} = w_i \sum_{n=0}^N \frac{1}{n!} \mathbf{a}^{(n)} : \mathcal{H}^{(n)}(\boldsymbol{\xi}_i). \quad (13)$$

Note that $\mathbf{a}^{(n)}$ can be accurately computed from Eq. (12) only up to $n = Q - N$. Equations (12) and (13) define an *isomorphic* transform between $\{\mathbf{a}^{(n)} : n = 0, \dots, N\}$ and $\{f_i : i = 1, \dots, d\}$, provided that the quadrature is sufficiently accurate, i.e., $Q \geq 2N$, and the distribution function is restricted to the finite-dimensional functional space spanned by the leading Hermite polynomials, i.e., that defined by Eq. (10). Note that the number of independent components in the leading $\mathbf{a}^{(n)}$ and the number of abscissas are not necessarily the same as the abscissas usually contain additional degrees of freedom from which some, but not all, components of moments beyond $Q - N$ could also be determined. These are the “ghost” moments which are neglected as they do not help raising the hydrodynamic order of the discrete scheme. Also to be noted is that the smaller of $Q - N$ and N determines

the order of moments that can be represented by the discrete velocities and hence, it is optimum to use a quadrature with $Q = 2N$.

The dynamic equations for f_i are obtained by directly evaluating Eq. (2) at $\boldsymbol{\xi}_i$. After space and time discretization, we can write the LBGK equation in the following form:

$$f_i(\mathbf{x} + \boldsymbol{\xi}_i, t + 1) = (1 - \omega) f_i + \omega f_i^{(0)}, \quad (14)$$

where $\omega \equiv 1/\tau$ is the collision frequency. Writing $f_i = f_i^{(0)} + f_i^{(1)}$ with $f_i^{(1)}$ being the *nonequilibrium* part of the distribution, the LBGK equation also has the equivalent form:

$$f_i(\mathbf{x} + \boldsymbol{\xi}_i, t + 1) = f_i^{(0)} + (1 - \omega) f_i^{(1)}. \quad (15)$$

B. Regularization and the general MRT model

Equations (12) and (13) also provide a natural decomposition of the discrete distribution, f_i , into components corresponding to the moments. Substituting Eq. (12) into Eq. (13), we have:

$$f_i = w_i \sum_{n=0}^N \frac{1}{n!} \mathcal{H}^{(n)}(\boldsymbol{\xi}_j) : \mathcal{H}^{(n)}(\boldsymbol{\xi}_i) f_j. \quad (16)$$

Einstein summation is assumed hereinafter, and the equation above holds if and only if f lies in the subspace spanned by the first N Hermite polynomials as give by Eq. (10). Defining the $d \times d$ projection matrices:

$$M_{ij}^{(n)} = \frac{w_i}{n!} \mathcal{H}^{(n)}(\boldsymbol{\xi}_i) : \mathcal{H}^{(n)}(\boldsymbol{\xi}_j), \quad (17)$$

$M_{ij}^{(n)} f_j$ is the component of f_j corresponding to the n th moment. Summing up the leading N components, we have the *regularization* operator $\hat{\cdot}$:

$$\hat{f}_i = \sum_{n=0}^N M_{ij}^{(n)} f_j, \quad (18)$$

which, when acted on an arbitrary set of f_i , trims the Hermite components higher than N and does nothing if f_i is already trimmed as in Eq. (16). A regularized BGK model similar to that of Ref. [10] can then be generally written as:

$$f_i(\mathbf{x} + \boldsymbol{\xi}_i, t + 1) = (1 - \omega) \hat{f}_i + \omega f_i^{(0)}. \quad (19)$$

The collision term on the right-hand side is characterized by three parameters: the collision frequency, ω , the projection order, N , and the truncation order of $f^{(0)}$, M , which is not necessarily the same as N . In case f_i contains no moments beyond the N th order, $\hat{f}_i = f_i$. Obviously, when $M \leq N$, we have:

$$\widehat{f_i^{(0)}} = f_i^{(0)}. \quad (20)$$

In that case, Eq. (19) can be written as:

$$f_i(\mathbf{x} + \boldsymbol{\xi}_i, t + 1) = f_i^{(0)} + (1 - \omega) \widehat{f_i^{(1)}}, \quad (21)$$

which is essentially an SRT regularized LB that discards all components of the distribution that correspond to moments higher than what can be accurately represented by f_i .

By assigning a separate relaxation time to each of the Hermite components of $f^{(1)}$, the previous MRT LB model

[14] can be written as:

$$f_i(\mathbf{x} + \boldsymbol{\xi}_i, t + 1) = f_i^{(0)} + \sum_{n=2}^N (1 - \omega_n) M_{ij}^{(n)} f_j^{(1)}, \quad (22)$$

where the summation starts from two because the zeroth and first moments of $f^{(1)}$ vanish due to mass and momentum conservation.

C. The multi-relaxation-time collision model

We now turn to the conditions for the collision operator to yield NSF equations by examining how the NSF equations are derived with the BGK collision model [35]. The hydrodynamic equations are the conservation laws of mass, momentum, and energy, all velocity moments. Taking these moments of Eq. (1), the right-hand side vanishes, and the left-hand side contains the following additional central moments:

$$\boldsymbol{\sigma} = \int f c c d\mathbf{c}, \quad \text{and} \quad \mathbf{q} = \frac{1}{2} \int f c^2 c d\mathbf{c}, \quad (23)$$

which are identified as the *pressure tensor* and *heat flux*. Here $\mathbf{c} \equiv \boldsymbol{\xi} - \mathbf{u}$ is the peculiar velocity. We need to express $\boldsymbol{\sigma}$ and \mathbf{q} in terms of ρ , \mathbf{u} , θ and their derivatives to close the conservation equations. At the zeroth order, f is taken to be the local Maxwellian of Eq. (3) which yields $\boldsymbol{\sigma}^{(0)} = \rho\theta\boldsymbol{\delta}$ and $\mathbf{q}^{(0)} = \mathbf{0}$, where $\boldsymbol{\delta}$ is the rank-2 identity tensor. On substituting into the conservation equations, we have Euler's equations. Next, on substituting $f = f^{(0)} + f^{(1)}$ into Eq. (1) and ignoring $f^{(1)}$ on the left-hand side, we have:

$$\left(\frac{\partial}{\partial t} + \boldsymbol{\xi} \cdot \nabla + \mathbf{g} \cdot \nabla_{\boldsymbol{\xi}} \right) f^{(0)} \cong -\omega f^{(1)}. \quad (24)$$

The first approximation, $f^{(1)}$, can be obtained after expressing the left-hand side in terms of ρ , \mathbf{u} , θ and their spatial derivatives by the chain rule of differentiation and the Euler's equation. Taking the corresponding moments, we have:

$$\sigma_{ij}^{(1)} = -\tau\rho\theta \left[\frac{\partial u_i}{\partial x_j} + \frac{\partial u_j}{\partial x_i} - \frac{2}{D} \delta_{ij} \nabla \cdot \mathbf{u} \right], \quad (25a)$$

$$\mathbf{q}^{(1)} = -\frac{D+2}{2} \tau\rho\theta \nabla\theta. \quad (25b)$$

On substituting the above into the conservation equations we have the NSF equations.

Evident from this procedure is that the form of the hydrodynamic equations is completely determined by $\boldsymbol{\sigma}^{(1)}$ and $\mathbf{q}^{(1)}$. As long as the collision term satisfies the following condition:

$$\int \Omega c^n d\mathbf{c} = -\omega_n \int f^{(1)} c^n d\mathbf{c}, \quad \text{for } n = 2, 3, \quad (26)$$

where $\boldsymbol{\sigma}^{(1)}$ and $\mathbf{q}^{(1)}$ will have the same form as Eqs. (25) with ω replaced by ω_2 and ω_3 respectively. The hydrodynamic equations will be the same NSF equations but with separately tunable viscosity and thermal diffusivity. More generally, it is natural to demand that Eq. (26) is satisfied for all n . This way, each of the CM's is relaxed at its own rate. Since the set of monomials, $\{c^n\}$, is a complete basis of the functional space, by specifying all moments of Ω , we specify Ω itself completely.

We now construct the collision operator in terms of its Hermite coefficients. Let the n th Hermite coefficients of Ω and $f^{(1)}$ in absolute frame be denoted by $\mathbf{a}_{\Omega}^{(n)}$ and $\mathbf{a}_1^{(n)}$, respectively, and those in the relative frame by $\mathbf{b}_{\Omega}^{(n)}$ and $\mathbf{b}_1^{(n)}$. Due to the conservations of mass and momentum, we must have $\mathbf{a}_1^{(0)} = \mathbf{a}_1^{(1)} = \mathbf{0}$ and hence $\mathbf{a}_{\Omega}^{(0)} = \mathbf{a}_{\Omega}^{(1)} = \mathbf{0}$. By Eqs. (A6a), we have $\mathbf{b}_1^{(0)} = \mathbf{b}_1^{(1)} = \mathbf{b}_{\Omega}^{(0)} = \mathbf{b}_{\Omega}^{(1)} = \mathbf{0}$, and

$$\mathbf{b}^{(2)} = \mathbf{a}^{(2)}, \quad (27a)$$

$$\mathbf{b}^{(3)} = \mathbf{a}^{(3)} - 3\mathbf{u}\mathbf{a}^{(2)}, \quad (27b)$$

$$\mathbf{b}^{(4)} = \mathbf{a}^{(4)} - 4\mathbf{u}\mathbf{a}^{(3)} + 6\mathbf{u}^2\mathbf{a}^{(2)}. \quad (27c)$$

The Hermite expansions of Ω and $f^{(1)}$ in the relative frame are as follows:

$$\Omega = \omega(\mathbf{c}) \sum_{n=2}^N \frac{1}{n!} \mathbf{b}_{\Omega}^{(n)} : \mathcal{H}^{(n)}(\mathbf{c}), \quad (28a)$$

$$f^{(1)} = \omega(\mathbf{c}) \sum_{n=2}^N \frac{1}{n!} \mathbf{b}_1^{(n)} : \mathcal{H}^{(n)}(\mathbf{c}). \quad (28b)$$

Writing \mathbf{c}^n in terms of $\mathcal{H}^{(n)}(\mathbf{c})$ by Eqs. (A3) and using the orthogonality relations, we have:

$$\int \Omega c^2 d\mathbf{c} = \mathbf{b}_{\Omega}^{(2)}, \quad (29a)$$

$$\int \Omega c^3 d\mathbf{c} = \mathbf{b}_{\Omega}^{(3)}, \quad (29b)$$

$$\int \Omega c^4 d\mathbf{c} = \mathbf{b}_{\Omega}^{(4)} + 6\delta\mathbf{b}_{\Omega}^{(2)}, \quad (29c)$$

and similar expressions for $\int f^{(1)} c^n d\mathbf{c}$. On substituting into Eq. (26), we arrive at a hierarchy of equations of which the leading few are

$$\mathbf{b}_{\Omega}^{(2)} = -\omega_2 \mathbf{b}_1^{(2)}, \quad (30a)$$

$$\mathbf{b}_{\Omega}^{(3)} = -\omega_3 \mathbf{b}_1^{(3)}, \quad (30b)$$

$$\mathbf{b}_{\Omega}^{(4)} + 6\delta\mathbf{b}_{\Omega}^{(2)} = -\omega_4 [\mathbf{b}_1^{(4)} + 6\delta\mathbf{b}_1^{(2)}]. \quad (30c)$$

Converting $\mathbf{b}^{(n)}$ to $\mathbf{a}^{(n)}$ using Eq. (27), we have:

$$\mathbf{a}_{\Omega}^{(2)} = -\omega_2 \mathbf{a}_1^{(2)}, \quad (31a)$$

$$\mathbf{a}_{\Omega}^{(3)} - 3\mathbf{u}\mathbf{a}_{\Omega}^{(2)} = -\omega_3 [\mathbf{a}_1^{(3)} - 3\mathbf{u}\mathbf{a}_1^{(2)}], \quad (31b)$$

$$\mathbf{a}_{\Omega}^{(4)} - 4\mathbf{u}\mathbf{a}_{\Omega}^{(3)} + 6(\mathbf{u}^2 + \delta)\mathbf{a}_{\Omega}^{(2)} = -\omega_4 [\mathbf{a}_1^{(4)} - 4\mathbf{u}\mathbf{a}_1^{(3)} + 6(\mathbf{u}^2 + \delta)\mathbf{a}_1^{(2)}]. \quad (31c)$$

Straightforwardly, $\mathbf{a}_{\Omega}^{(n)}$ can be solved as:

$$\mathbf{a}_{\Omega}^{(2)} = -\omega_2 \mathbf{a}_1^{(2)}, \quad (32a)$$

$$\mathbf{a}_{\Omega}^{(3)} = -\omega_3 \mathbf{a}_1^{(3)} + 3(\omega_3 - \omega_2) \mathbf{u}\mathbf{a}_1^{(2)}, \quad (32b)$$

$$\mathbf{a}_{\Omega}^{(4)} = -\omega_4 \mathbf{a}_1^{(4)} + 4(\omega_4 - \omega_3) \mathbf{u}\mathbf{a}_1^{(3)} - 6[(\omega_4 + \omega_2 - 2\omega_3)\mathbf{u}^2 + (\omega_4 - \omega_2)\delta]\mathbf{a}_1^{(2)}, \quad (32c)$$

which are the Hermite coefficients of Ω in the absolute frame. For comparison, the similar coefficients of the BGK and the

high-order MRT [14] operators are, respectively:

$$\mathbf{a}_\Omega^{(n)} = -\omega \mathbf{a}_1^{(n)}, \quad \text{and} \quad \mathbf{a}_\Omega^{(n)} = -\omega_n \mathbf{a}_1^{(n)}. \quad (33)$$

We first note that when all the relaxation times are the same, all three are identical. Second, as far as the second moments are concerned, relaxations of the central and raw moments are equivalent. This is in agreement with some of the numerical observation [26]. Third, the correction to the third moments, i.e., the second term on the right-hand side of Eq. (32b), recovers the result in Ref. [15].

The computation of the collision process goes as the following. Given the poststreaming distribution, f_i , its nonequilibrium part is $f_i^{(1)} = f_i - f_i^{(0)}$, from which $\mathbf{a}_1^{(n)}$, and $\mathbf{a}_\Omega^{(n)}$ in turn, can be calculated by Eqs. (12) and (32). Ω_i is then obtained from $\mathbf{a}_\Omega^{(n)}$ using Eq. (13), and, finally, the postcollision distribution is updated using the following lattice Boltzmann equation:

$$f_i(\mathbf{x} + \boldsymbol{\xi}_i, t + 1) = \hat{f}_i + \Omega_i. \quad (34)$$

III. NUMERICAL VERIFICATION

In this section we numerically verify the CM-based MRT (CM-MRT) model. First, the viscosity and thermal diffusivity were numerically measured *via* the dynamics of the linear hydrodynamic modes in the presence of a translational flow. The numerical measurements are then compared with theoretical values. The independence of the transport coefficients on the translational flow, and hence the Galilean invariance in the dissipation terms, can then be verified. Second, a thorough and complete characterization of CM-MRT's numerical stability is beyond the scope of the present paper and deferred to a later publication. Here we choose to only present some preliminary results on the popular test case of the double shear layer [43,44]. The results seem to show that the CM-MRT is at least as stable as the regularized collision models.

A. Linear hydrodynamic modes test

We first summarize the theoretical predictions of the viscous, thermal, and acoustic modes in the presence of a translational flow. Consider a small monochromatic perturbations on top of a base flow with constant velocity. The density, velocity, and temperature, all nondimensionalized by the scheme in Ref. [33], are as follows:

$$\rho = \rho_0 + \rho', \quad \mathbf{u} = \mathbf{u}_0 + \mathbf{u}', \quad \text{and} \quad \theta = \theta_0 + \theta'. \quad (35)$$

where the subscript $_0$ and the primes denote the quantities of the base flow and the perturbation, respectively. The perturbations are in the form of:

$$\begin{pmatrix} \rho' \\ \mathbf{u}' \\ \theta' \end{pmatrix} = \begin{pmatrix} \tilde{\rho} \\ \tilde{\mathbf{u}} \\ \tilde{\theta} \end{pmatrix} e^{\omega t + i\mathbf{k} \cdot (\mathbf{x} - \mathbf{u}_0 t)}, \quad (36)$$

where $\tilde{\rho}$, $\tilde{\mathbf{u}}$, and $\tilde{\theta}$ are constant amplitudes; ω and \mathbf{k} the frequency and wave vector; and \mathbf{x} the spatial coordinate. Decomposing $\tilde{\mathbf{u}}$ into components parallel and perpendicular to the wave vector, \tilde{u}_\parallel and \tilde{u}_\perp , respectively, by writing $\tilde{\mathbf{u}} = \tilde{u}_\parallel \mathbf{e}_\parallel + \tilde{u}_\perp \mathbf{e}_\perp$, where \mathbf{e}_\parallel and \mathbf{e}_\perp are unit vectors parallel and perpendicular to \mathbf{k} , on substituting Eqs. (35) and (36) into the NSF equations, we arrive at an eigensystem in the linear space of $(\tilde{\rho}, \tilde{u}_\parallel, \tilde{\theta}, \tilde{u}_\perp)^T$. The four eigenvalues give the dispersion

relations, while the eigenvectors define the corresponding amplitudes [45]. Let γ be the *heat capacity ratio*, ν and η the first and second *kinematic viscosities*, and κ the thermal diffusivity. Defining the *acoustic Reynolds* and *Péclet numbers* as $\text{Re} = c_s/\nu k$ and $\text{Pe} = c_s/\kappa k$, where $c_s \equiv \sqrt{\gamma\theta_0}$ is the *sound speed* at temperature θ_0 , Re and Pe are related by $\text{Pe} = \text{Re} \cdot \text{Pr}$, where $\text{Pr} \equiv \nu/\kappa$ is the Prandtl number. The theoretical dimensionless dispersion relations of the viscous, thermal, and acoustic modes are as follows:

$$-\frac{\omega_v}{c_s k} = \frac{1}{\text{Re}}, \quad (37a)$$

$$-\frac{\omega_t}{c_s k} = \frac{1}{\text{Pe}} + \frac{(\gamma - 1)\lambda}{\text{Pe}^3} + \mathcal{O}\left(\frac{1}{\text{Pe}^5}\right), \quad (37b)$$

$$-\frac{\omega_\pm}{c_s k} = \frac{\gamma - \lambda}{2\text{Pe}} - \frac{(\gamma - 1)\lambda}{2\text{Pe}^3} + \mathcal{O}\left(\frac{1}{\text{Pe}^5}\right) \pm i \left[1 - \frac{(\gamma + \lambda)^2 - 4\lambda}{8\text{Pe}^2} + \mathcal{O}\left(\frac{1}{\text{Pe}^4}\right) \right], \quad (37c)$$

where ω_v , ω_t , and ω_\pm are the corresponding angular frequencies and $\lambda \equiv 1 + (\gamma - 3)\text{Pr}$. Note that while the dispersion relation of the viscous mode is exact, the other three are solutions of a cubic *characteristic equation* and only their asymptotic expansions at the small-Pe limit are given.

The numerical measurements were carried out as the following. First, given the desired amplitudes of the four modes, the initial perturbation, ρ' , \mathbf{u}' , and θ' , were constructed using Eqs. (36) as a superposition of the eigenmodes. Subsequent amplitudes were determined by performing a spatial Fourier transform on a corresponding data field to extract the amplitude of the given wave number. Noting that sound propagation is isentropic and thermal diffusion is isobaric, the data fields for the viscous, thermal, and acoustic modes are u_\perp , the entropy $s \equiv c_v \ln(\theta \rho^{1-\gamma})$, and the pressure, $p \equiv \rho\theta$, respectively.

Shown in Fig. 1 are the typical time histories of the linear mode amplitudes measured numerically. The CM-MRT model with a ninth-order 37-speed quadrature was used. The simulation was performed with $\nu = 0.1$ and $\kappa = 0.2$, yielding a Prandtl number of 0.5. The density, temperature, and translational velocity of the base flow are $\rho_0 = 1$, $\theta_0 = 1.2$, and $\mathbf{u}_0 = \mathbf{0}$. The initial perturbation consisted of a superposition of three monochrome viscous, thermal, and standing acoustic waves, all with amplitude 0.001 and wave number (1,0), (1,1), and (1,0), respectively. The time histories were fitted with the theoretical model of Eq. (36) to determine the angular frequencies. Comparing with Eqs. (37), the errors in ω_v , ω_t and the real and imaginary parts of ω_\pm are respectively 0.17%, 0.19%, 0.19%, and 0.01%.

Using this measurement mechanism, we first tested the grid convergence of the CM-MRT model with a number of high-order quadratures. As previously shown [42], high-order quadrature rules with abscissas coincide with lattice nodes (on-lattice) can be found by solving a linear programming problem. The solutions form an polytope in the parameter space of which the vertexes represent the quadrature rules with minimum number of velocities. In two dimensions, the minimum seventh-degree rules are the four $E_{2,17}^7$ rules, and the minimum ninth-degree rules are the four $E_{2,37}^9$ rules, all

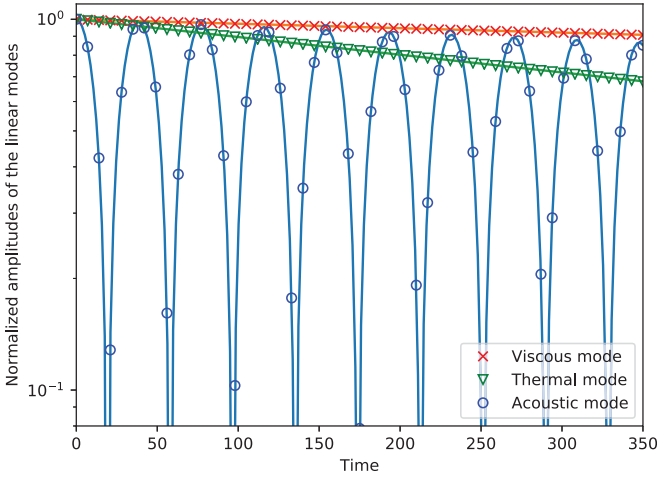


FIG. 1. Typical time histories of the linear mode amplitudes. The simulation was performed on a 100×100 double periodic lattice. Shown are the absolute values of the amplitudes of the viscous, thermal, and standing acoustic waves all normalized with their initial values. The solid lines are theoretical results and symbols numerical measurements.

given in Ref. [42]. These two classes of rules are capable of accurately representing moments up to the third and fourth orders, respectively. Shown in Fig. 2 are the relative errors in viscosity and thermal diffusivity as measured by the linear mode tests using the CM-MRT model with all eight quadratures. Hereinafter the relative error of a quantity, φ , is defined as $\varphi^* \equiv |\varphi_n - \varphi_t|/\varphi_t$ with φ_n and φ_t being the numerical and theoretical values. All models demonstrate a second-order spatial accuracy with the one using quadrature $E_{2,17}^7$ -D being the most accurate.

We then verify the dependence of the sound speed on the temperature by measuring the relative error with respect to the theoretical value of Eq. (37c). We set $\nu = \kappa = 0.01$ and only enable a monochrome sound wave in the initial condition. The measured relative error in sound speed is plotted in Fig. 3 vs the dimensionless temperature θ_0 . The accuracy of sound speed dependence on the temperature is in the order of 10^{-4} .

We then used this apparatus to verify the Galilean invariance by including a translational velocity in the base flow, in a similar fashion as in Ref. [15]. Specifically we set $\mathbf{u}_0 = (0, u_0)$, and the initial perturbation consists of a viscous and a thermal wave, both with wave vector $\mathbf{k} = (1, 0)$ and initial amplitude of 0.001. The base flow is in the transverse direction of the wave vector. Shown in Fig. 4 are the relative errors in viscosity, thermal diffusivity, and speed sound against u_0 using the MRT [14] and CM-MRT models. To be seen is that viscosity and sound speed are Galilean invariant for both models, while the thermal diffusivity linearly depends on u_0 , in agreement with Eq. (32b). This violation of Galilean invariance is eliminated in CM-MRT.

B. Double shear layer test

The double-shear-layer (DSL) [43,44] is a well-studied test case for numerical stability benchmark [12,13,46–49]. The

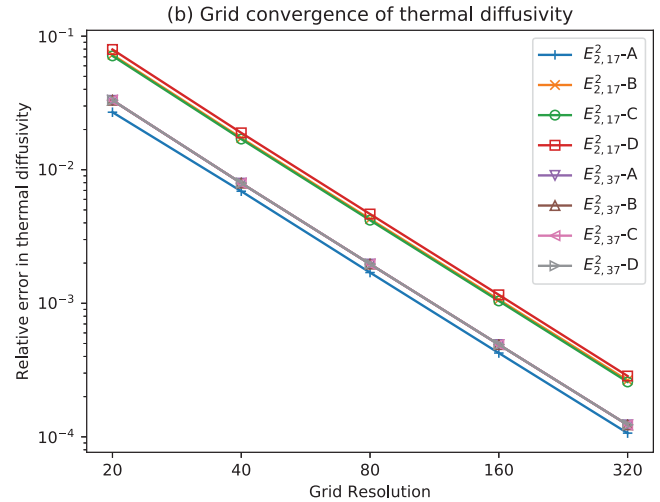
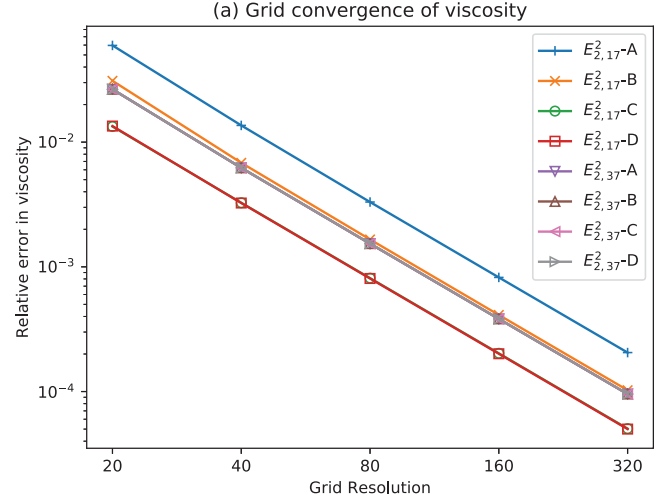


FIG. 2. Grid convergence of the CM-MRT model. Plotted are the relative errors in viscosity (top) and thermal diffusivity (bottom) using the $E_{2,17}^7$ and $E_{2,37}^9$ quadratures on a $L \times L$ lattice ranging from $L = 20$ to $L = 320$. The errors in viscosity of the four $E_{2,37}^9$ quadrature are almost identical and coincide on the graph. Although all models are second order, the magnitudes of the error can differ by a factor of approximately 4 to 5. The quadrature $E_{2,17}^7$ -D is found to have the best accuracy.

two-dimensional flow field is defined on a double periodic domain $0 \leq x, y \leq 1$ by:

$$u_x = \begin{cases} u_0 \tanh \rho(y - \frac{1}{4}), & y \leq \frac{1}{2} \\ u_0 \tanh \rho(\frac{3}{4} - y), & y > \frac{1}{2} \end{cases}, \quad (38a)$$

$$u_y = \delta u_0 \sin 2\pi[x + \frac{1}{4}], \quad (38b)$$

where $1/\rho$ measures the thickness of the shear layer, and δ a small parameter controlling the magnitude of the initial vertical perturbation. In simulations here, we chose $\rho = 80$ and $\delta = 0.05$ in accordance with the literature. All simulations are performed on a $L \times L$ square lattice where L is the number of sites in one direction. In our notation [33], lengths are scaled by the lattice constant, c , and velocities by the

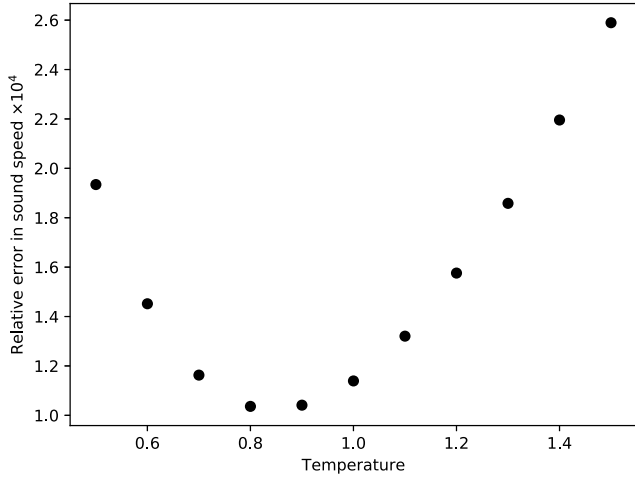


FIG. 3. Relative error in the numerically measured sound speed against its theoretical value for a range of temperature. To be seen is that the error is less than 3×10^{-4} for the range of temperature $0.5 < \theta_0 < 1.5$. To ensure the sound wave is isotropic with respect to the grid, the measurement was conducted on a 108×261 lattice with wave numbers (1, 1) so that the wave vector forms an angle of approximately $\pi/8$ with the horizontal axis. The $E_{2,37}^9$ -A quadrature rule is used.

isothermal sound speed, c_s . The Reynolds and Mach numbers are therefore $Re = u_0 cL/\nu$ and $Ma = u_0$.

Extensive studies on the DSL were carried out to benchmark various collision models [12,13]. For comparison, we also computed the stability boundary of the DSL using the isothermal MRT, isothermal CM-MRT and full thermal CM-MRT models on the same $L = 128$ lattice. For a fixed pair of Pr and Re , the maximum Ma is defined as the highest Ma that allows the simulation to be stably carried out to $t/t_c = 2$

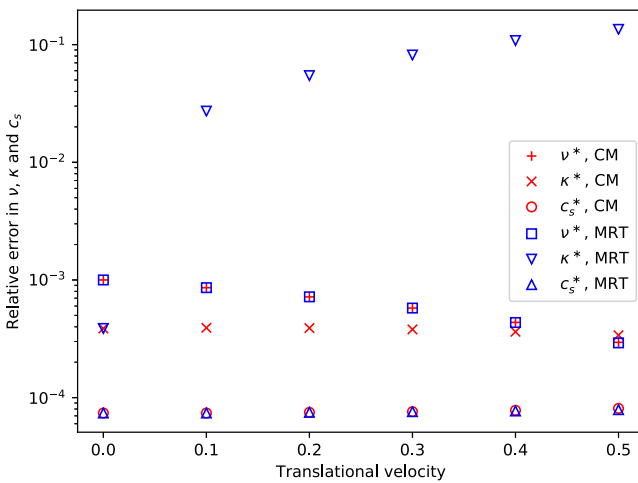


FIG. 4. Galilean invariance of the transport coefficients by the CM-MRT model. Plotted are the relative errors in viscosity, ν^* , thermal diffusivity, κ^* , and sound speed, c_s^* , as measured by the linear-mode tests using MRT and CM-MRT, both with the $E_{2,37}^9$ quadrature on a 100×100 lattice. On the horizontal axis is the magnitude of the translational velocity. The error in thermal diffusivity in the MRT model increases with u_0 , breaking the Galilean invariance.

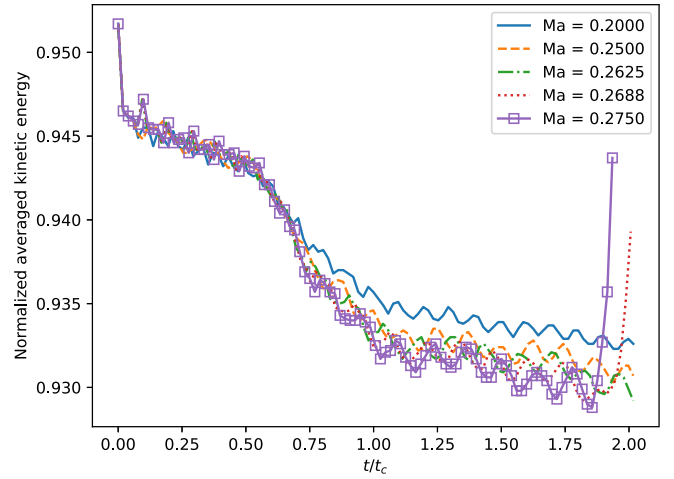


FIG. 5. Time histories of the averaged kinetic energy normalized by its initial value for a sequence of Mach number at $Pr = 1$ and $Re = 10^7$ using thermal CM-MRT on an 128×128 lattice. At $Ma = 0.275$ the simulation diverged and at 0.2688 it barely survived beyond $t/t_c = 2$.

[13]. An iterative search algorithm was used to find the maximum Ma for fixed Pr and Re . Shown in Fig. 5 are the time histories of the averaged kinetic energy, $\langle u^2 \rangle / u_0^2$, for an increasing sequence of Mach numbers at $Pr = 1$ and $Re = 10^7$ using the thermal CM-MRT. The maximum Ma is determined at 0.2688 in this case.

Shown in Fig. 6 are the stability boundaries in the Re - Ma plane using, from top to bottom, isothermal MRT, isothermal CM-MRT, and full thermal CM-MRT models. The same $E_{2,37}^9$ -A quadrature was used in all cases and the truncation levels were $M = N = 4$. In the isothermal cases, the temperature field was frozen at unity so that heat transfer is not simulated and τ_3 becomes a free parameter with no direct impact on the hydrodynamic equations. To study its effect on numerical stability, the stability boundaries are plotted for a range of Prandtl numbers defined as $Pr \equiv \nu/\kappa$. It is evident from Fig. 6 that for the isothermal simulations with τ_3 not too far from τ_2 , the MRT and CM-MRT perform similarly in terms of achievable Mach number and Reynolds number. Comparing with the best result of the regularized LBGK models [12,13], the present result ($Ma \sim 0.7$) is approximately 20% better. For comparison, in the full thermal case, the maximum achievable Ma number drops to ~ 0.25 over a wide range of Prandtl number. Nevertheless, taking into account that the grid is severely under-resolved, this maximum is by no means implied as a limit in practical simulations. Shown in Figs. 7 and 8 are the grayscale plots of the vorticity field at $t/t_c = 2$ corresponding to the middle graph in Fig. 6. The Mach numbers are 0.7 (Fig. 7) and 0.65 (8), respectively. Although the flow field has exhibited significant small-scale oscillations at $Ma = 0.7$, to be consistent with the aforementioned criterion, these cases are accepted as stable.

IV. CONCLUSIONS AND DISCUSSION

In summary, we propose a general high-order LB collision model which corrects the non-Galilean-invariant thermal

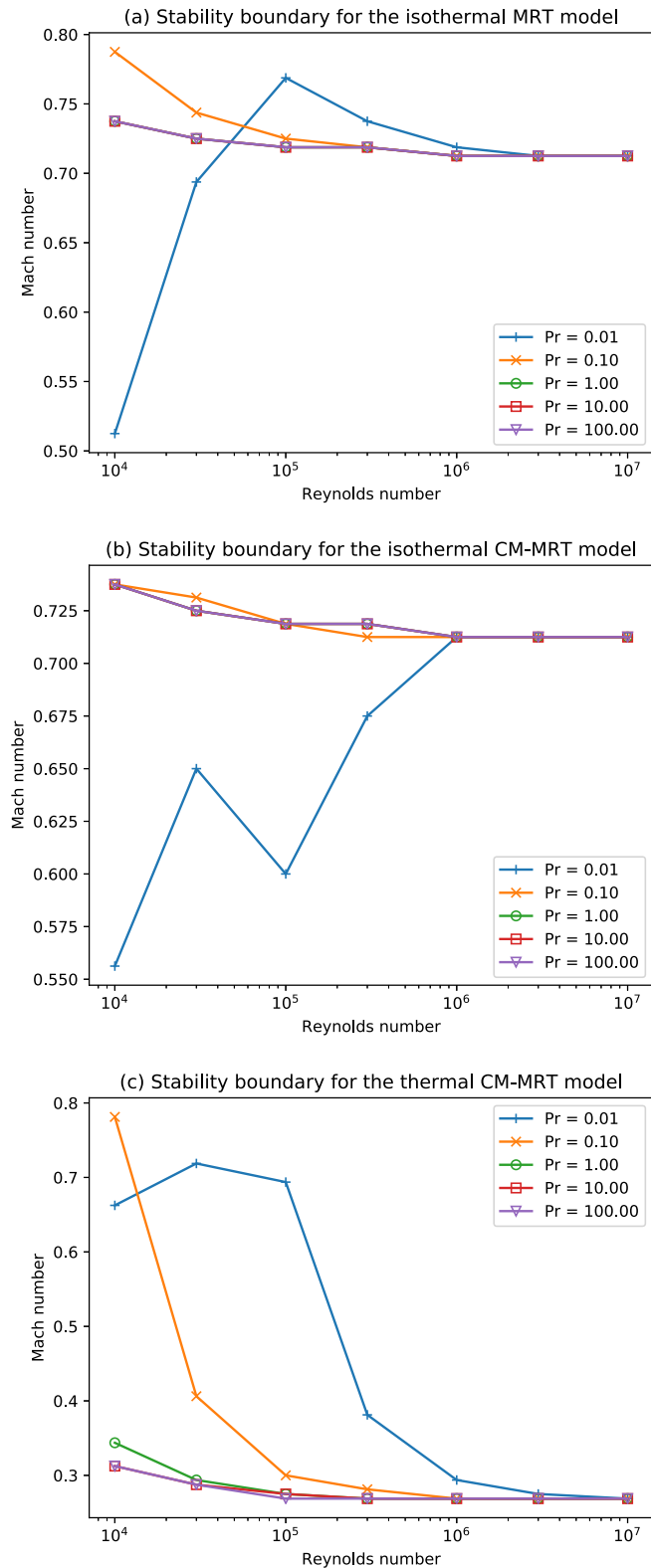


FIG. 6. Stability boundaries in the double-shear-layer simulation using isothermal MRT (top), isothermal CM-MRT (middle), and thermal CM-MRT (bottom) models. On the y axis is the maximum Mach number (u_0) that the simulation can be carried out to $u_0 t / Lc = 2$. For comparison, the Prandtl number is used as a measure of τ_3 relative to τ_2 in the top two isothermal cases although heat transfer is not simulated there.

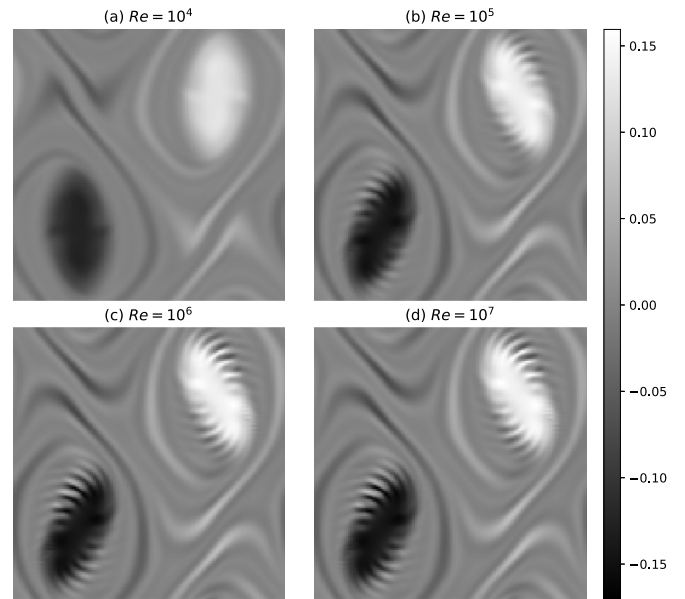


FIG. 7. Grayscale plot of the vorticity field at $t/t_c = 2$ in isothermal simulation using $E_{2,37}^9$ quadrature and CM-MRT model. The Mach number is 0.7, $Pr = 1$, and the Re is, from left to right and top to bottom, 10^4 , 10^5 , 10^6 , and 10^7 , respectively, corresponding to the middle graph in Fig. 6, right below the stability boundary. The vorticity fields show significant energy pile-up in the small scale for all Re except 10^4 , indicating severely insufficient resolution and poor accuracy.

diffusivity of the previous work [14]. The model is constructed by relaxing the central moments with separate relaxation rates and then converting them back to the absolute frame via binomial transform to preserve the streaming-collision

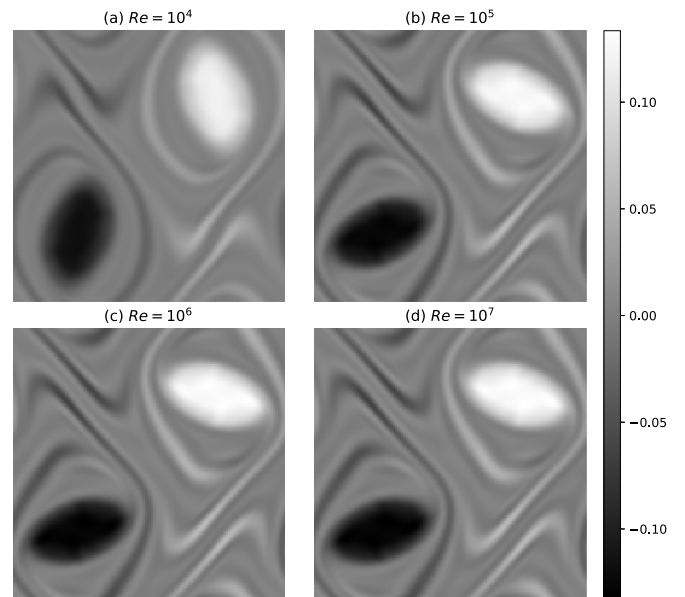


FIG. 8. Grayscale plot of the vorticity field at $t/t_c = 2$ in isothermal simulation. Otherwise identical to Fig. 7 except that the Mach number is 0.65. The small-scale oscillations are absent at this lower Mach number.

algorithm. The construction of the model guarantees that Chapman-Enskog calculation yields correct hydrodynamic equations with independent transport coefficients. It is theoretically shown and numerically verified that both viscous and thermal dissipation are Galilean invariant. The derivation is simple, lattice independent, and applicable to any order. Excellent numerical stability was also observed in the double-shear-layer test. For future exploration, we point out that the present collision model is fully specified by a spectrum of relaxation rates. While the leading two correspond to the viscosity and thermal diffusivity, the physical meanings of the higher relaxation rates are unclear. The determination of them might open new possibilities in modeling nonequilibrium flows and/or improving numerical stability.

ACKNOWLEDGMENTS

This work was supported by the National Natural Science Foundation of China Grants No. 91741101 and No. 91752204 and Science and Technology Innovation Committee Foundation of Shenzhen Grant No. JCYJ20170817105533245.

APPENDIX: HERMITE EXPANSIONS IN THE ABSOLUTE AND RELATIVE FRAMES

The tensorial Hermite polynomials can be defined by the recursive relation:

$$\xi \mathcal{H}^{(n)}(\xi) = \mathcal{H}^{(n+1)}(\xi) + n\delta \mathcal{H}^{(n-1)}(\xi), \quad (\text{A1})$$

where δ is the rank-2 identity tensor. The first few are as follows:

$$\mathcal{H}^{(0)}(\xi) = 1, \quad (\text{A2a})$$

$$\mathcal{H}^{(1)}(\xi) = \xi, \quad (\text{A2b})$$

$$\mathcal{H}^{(2)}(\xi) = \xi^2 - \delta, \quad (\text{A2c})$$

$$\mathcal{H}^{(3)}(\xi) = \xi^3 - 3\xi\delta, \quad (\text{A2d})$$

$$\mathcal{H}^{(4)}(\xi) = \xi^4 - 6\xi^2\delta + 3\delta^2. \quad (\text{A2e})$$

Inversely, the monomials can be expressed by the Hermite polynomials:

$$1 = \mathcal{H}^{(0)}(\xi), \quad (\text{A3a})$$

$$\xi = \mathcal{H}^{(1)}(\xi), \quad (\text{A3b})$$

$$\xi^2 = \mathcal{H}^{(2)}(\xi) + \delta \mathcal{H}^{(0)}(\xi), \quad (\text{A3c})$$

$$\xi^3 = \mathcal{H}^{(3)}(\xi) + 3\delta \mathcal{H}^{(1)}(\xi), \quad (\text{A3d})$$

$$\xi^4 = \mathcal{H}^{(4)}(\xi) + 6\delta \mathcal{H}^{(2)}(\xi) + 3\delta^2 \mathcal{H}^{(0)}(\xi). \quad (\text{A3e})$$

In statistics, the *central* and *raw* moments of a distribution, defined as the moments about the mean and origin, respectively, are related to each other by the *binomial transform*. Similar relations exist between the Hermite polynomials and the expansion coefficients in the relative and absolute reference frames. First, the following relation can be established by induction:

$$\mathcal{H}^{(n)}(\xi + \mathbf{u}) = \sum_{i=0}^n C_n^i \mathcal{H}^{(i)}(\xi) \mathbf{u}^{n-i}, \quad (\text{A4})$$

where C_n^i is the *binomial coefficient*. The Hermite polynomials in the relative and absolute frames are hence related to each other by the following binomial transforms:

$$\mathcal{H}^{(n)}(\mathbf{c}) = \sum_{i=0}^n (-1)^{n-i} C_n^i \mathcal{H}^{(i)}(\xi) \mathbf{u}^{n-i}, \quad (\text{A5a})$$

$$\mathcal{H}^{(n)}(\xi) = \sum_{i=0}^n C_n^i \mathcal{H}^{(i)}(\mathbf{c}) \mathbf{u}^{n-i}, \quad (\text{A5b})$$

where $\mathbf{c} \equiv \xi - \mathbf{u}$. Let $\mathbf{a}^{(n)}$ and $\mathbf{b}^{(n)}$ be respectively the Hermite coefficients in the absolute and relative frames. By Eq. (8), they are related to each other by the binomial transforms:

$$\mathbf{b}^{(n)} = \sum_{i=0}^n (-1)^{n-i} C_n^i \mathbf{a}^{(i)} \mathbf{u}^{n-i}, \quad (\text{A6a})$$

$$\mathbf{a}^{(n)} = \sum_{i=0}^n C_n^i \mathbf{b}^{(i)} \mathbf{u}^{n-i}. \quad (\text{A6b})$$

Explicitly, the leading few expressions are

$$\mathbf{b}^{(0)} = \mathbf{a}^{(0)}, \quad (\text{A7a})$$

$$\mathbf{b}^{(1)} = \mathbf{a}^{(1)} - \mathbf{u} \mathbf{a}^{(0)}, \quad (\text{A7b})$$

$$\mathbf{b}^{(2)} = \mathbf{a}^{(2)} - 2\mathbf{u} \mathbf{a}^{(1)} + \mathbf{u}^2 \mathbf{a}^{(0)}, \quad (\text{A7c})$$

$$\mathbf{b}^{(3)} = \mathbf{a}^{(3)} - 3\mathbf{u} \mathbf{a}^{(2)} + 3\mathbf{u}^2 \mathbf{a}^{(1)} - \mathbf{u}^3 \mathbf{a}^{(0)}, \dots, \quad (\text{A7d})$$

and

$$\mathbf{a}^{(0)} = \mathbf{b}^{(0)}, \quad (\text{A8a})$$

$$\mathbf{a}^{(1)} = \mathbf{b}^{(1)} + \mathbf{u} \mathbf{b}^{(0)}, \quad (\text{A8b})$$

$$\mathbf{a}^{(2)} = \mathbf{b}^{(2)} + 2\mathbf{u} \mathbf{b}^{(1)} + \mathbf{u}^2 \mathbf{b}^{(0)}, \quad (\text{A8c})$$

$$\mathbf{a}^{(3)} = \mathbf{b}^{(3)} + 3\mathbf{u} \mathbf{b}^{(2)} + 3\mathbf{u}^2 \mathbf{b}^{(1)} + \mathbf{u}^3 \mathbf{b}^{(0)}, \dots \quad (\text{A8d})$$

- [1] U. Frisch, B. Hasslacher, and Y. Pomeau, *Phys. Rev. Lett.* **56**, 1505 (1986).
 [2] R. Benzi, S. Succi, and M. Vergassola, *Phys. Rep.* **222**, 145 (1992).
 [3] S. Chen and G. D. Doolen, *Annu. Rev. Fluid Mech.* **30**, 329 (1998).
 [4] P. Bhatnagar, E. P. Gross, and M. Krook, *Phys. Rev.* **94**, 511 (1954).
 [5] H. Chen, S. Chen, and W. H. Matthaeus, *Phys. Rev. A* **45**, R5339(R) (1992).

- [6] Y.-H. Qian, D. D'Humières, and P. Lallemand, *Europhys. Lett.* **17**, 479 (1992).
 [7] D. d'Humières, in *Rarefied Gas Dynamics: Theory and Simulations*, Progress in Astronautics and Aeronautics, Vol. 159, edited by B. D. Shizgal and D. P. Weaver (American Institute of Aeronautics and Astronautics (AIAA), Washington DC, 1992), pp. 450–458.
 [8] D. d'Humières, I. Ginzburg, M. Krafczyk, P. Lallemand, and L.-S. Luo, *Philos. Trans. R. Soc. Lond. A* **360**, 437 (2002).

- [9] M. Geier, A. Greiner, and J. G. Korvink, *Phys. Rev. E* **73**, 066705 (2006).
- [10] J. Latt and B. Chopard, *Math. Comput. Simul.* **72**, 165 (2006).
- [11] H. Chen, R. Zhang, I. Staroselsky, and M. Jhon, *Phys. A Stat. Mech. Appl.* **362**, 125 (2006).
- [12] K. K. Mattila, P. C. Philippi, and L. A. Hegele, *Phys. Fluids* **29**, 046103 (2017).
- [13] C. Coreixas, G. Wissocq, G. Puigt, J.-F. Boussuge, and P. Sagaut, *Phys. Rev. E* **96**, 033306 (2017).
- [14] X. Shan and H. Chen, *Int. J. Mod. Phys. C* **18**, 635 (2007).
- [15] H. Chen, P. Gopalakrishnan, and R. Zhang, *Int. J. Mod. Phys. C* **25**, 1450046 (2014).
- [16] E. P. Gross and E. A. Jackson, *Phys. Fluids* **2**, 432 (1959).
- [17] L. H. Holway, *Phys. Fluids* **9**, 1658 (1966).
- [18] P. Andries, in *Rarefied Gas Dynamics: 22nd International Symposium*, edited by T. J. Bartel and M. A. Gallis, AIP Conf. Proc. No. 585 (AIP, New York, 2001).
- [19] E. M. Shakhov, *Fluid Dyn.* **3**, 95 (1968).
- [20] G. R. McNamara, A. L. Garcia, and B. J. Alder, *J. Stat. Phys.* **87**, 1111 (1997).
- [21] Y. Chen, H. Ohashi, and M. Akiyama, *Phys. Rev. E* **50**, 2776 (1994).
- [22] X. Nie, X. Shan, and H. Chen, *Europhys. Lett.* **81**, 34005 (2008).
- [23] Y.-H. Qian and S. A. Orszag, *Europhys. Lett.* **21**, 255 (1993).
- [24] P. J. Dellar, *J. Comput. Phys.* **259**, 270 (2014).
- [25] G. Kaehler and A. J. Wagner, *Phys. Rev. E* **87**, 063310 (2013).
- [26] Y. Ning, K. N. Premnath, and D. V. Patil, *Int. J. Numer. Methods Fluids* **82**, 59 (2016).
- [27] L. Fei, K. H. Luo, C. Lin, and Q. Li, *Int. J. Heat Mass Transf.* **120**, 624 (2018).
- [28] G. R. McNamara, A. L. Garcia, and B. J. Alder, *J. Stat. Phys.* **81**, 395 (1995).
- [29] O. Malaspinas, arXiv:1505.06900 (2015).
- [30] C. Sun, *J. Comput. Phys.* **161**, 70 (2000).
- [31] C. Sun and A. T. Hsu, *Phys. Rev. E* **68**, 016303 (2003).
- [32] X. Shan and X. He, *Phys. Rev. Lett.* **80**, 65 (1998).
- [33] X. Shan, X.-F. Yuan, and H. Chen, *J. Fluid Mech.* **550**, 413 (2006).
- [34] S. Chapman and T. G. Cowling, *The Mathematical Theory of Non-Uniform Gases*, 3rd ed. (Cambridge University Press, London, 1970).
- [35] K. Huang, *Statistical Mechanics*, 2nd ed. (John Wiley & Sons, New York, 1987).
- [36] H. Grad, *Commun. Pure Appl. Math.* **2**, 325 (1949).
- [37] V. I. Krylov, *Approximate Calculation of Integrals* (MacMillan, New York, 1962).
- [38] A. H. Stroud, *Approximate Calculation of Multiple Integrals* (Prentice-Hall, Englewood Cliffs, NJ, 1971).
- [39] P. C. Philippi, L. A. Hegele, Jr., L. O. E. dos Santos, and R. Surmas, *Phys. Rev. E* **73**, 056702 (2006).
- [40] S. S. Chikatamarla and I. V. Karlin, *Phys. Rev. E* **79**, 046701 (2009).
- [41] X. Shan, *Phys. Rev. E* **81**, 036702 (2010).
- [42] X. Shan, *J. Comput. Sci.* **17**, 475 (2016).
- [43] D. L. Brown and M. L. Minion, *J. Comput. Phys.* **122**, 165 (1995).
- [44] M. L. Minion and D. L. Brown, *J. Comput. Phys.* **138**, 734 (1997).
- [45] Y. Li and X. Shan, *Philos. Trans. R. Soc. Lond. A* **369**, 2371 (2011).
- [46] P. J. Dellar, *Phys. Rev. E* **64**, 031203 (2001).
- [47] P. J. Dellar, *J. Comput. Phys.* **190**, 351 (2003).
- [48] F. Bösch, S. S. Chikatamarla, and I. V. Karlin, *ESAIM Proc. Surv.* **52**, 1 (2015).
- [49] K. K. Mattila, L. A. Hegele, and P. C. Philippi, *Phys. Rev. E* **91**, 063010 (2015).